NANOSYSTEMS:
PHYSICS, CHEMISTRY, MATHEMATICS

Original article

Gorbenko O.M., et al. *Nanosystems: Phys. Chem. Math.*, 2024, **15** (5), 643–653.
http://nanojournal.ifmo.ru
DOI 10.17586/2220-8054-2024-15-5-643-653

Inertial nanostep piezoelectric drive: modeling and experiment

Olga M. Gorbenko[1,a], Stanislav Y. Lukashenko[1,b], Stepan V. Pichakhchi[1,2,c], Ivan D. Sapozhnikov[1,d], Mikhail L. Felshtyn[1,e], Alexander O. Golubok[1,2,f]

[1]Institute for Analytical Instrumentation of RAS, St. Petersburg, Russia
[2]St. Petersburg Academic University, St. Petersburg, Russia

[a]gorolga64@gmail.com, [b]lukashenko13@mail.ru, [c]pichakhchi.s@yandex.ru,
[d]sapojnikov@gmail.com, [e]mfelsztyn@yandex.ru, [f]aogolubok@mail.ru

Corresponding author: O.M. Gorbenko gorolga64@gmail.com

ABSTRACT A vertical inertial nanostep piezoelectric drive is considered. A virtual model was created, and the operating modes of a real drive were studied by numerical experiment. Piezo electromechanical resonance was discovered and a method to eliminate resonant vibrations by increasing electrical losses in the discharge circuit of the piezo actuator capacitance was proposed. A satisfactory agreement between the calculated and experimental data for the drive steps in the nanometer displacement range was obtained.

KEYWORDS inertial piezoelectric drive, nano positioning system, piezo actuator, piezoelectric effect

FOR CITATION Gorbenko O.M., Lukashenko S.Y., Pichakhchi S.V., Sapozhnikov I.D., Felshtyn M.L., Golubok A.O. Inertial nanostep piezoelectric drive: modeling and experiment. *Nanosystems: Phys. Chem. Math.*, 2024, **15** (5), 643–653.

1. Introduction

Due to the development of nanotechnology, precision mechanical scanning, positioning and manipulating systems with nanometer accuracy are of great interest. There are various approaches to the implementation of nano movements based on the use of purely mechanical systems, such as a lever, differential screw or a "soft spring-rigid membrane" type gearbox, as well as systems based on electromagnetic and piezoelectric nano drives. The nanometer step value imposes special requirements on their protection of such systems from thermal drifts, acoustic, mechanical and electromagnetic noise. In some cases, there are also restrictions for the size of nano movement systems and special requirements for their operating conditions (low temperatures, ultrahigh vacuum). In this regard, piezoelectric drives are of particular interest [1–4]. Indeed, since piezoelectric actuators (PA) generate small mechanical displacements in the range of 1 – 100 microns, positioning and manipulation systems based on them have high accuracy of $\sim 1 - 10$ nm, and due to the fact that in PA the energy of the electric field is directly converted into mechanical displacement, they are simple, compact and relatively high rigidity and, as a result, they have good protection against thermal drift and external mechanical vibrations. Piezoelectric drives are usually divided into three groups: resonant drives in which vibrations in the ultrasonic frequency range are transmitted through a friction coupling to a moving element [5–10], stepper drives operating in a quasi-static mode when the drive supports are alternately pressed against a fixed base during compression/stretching of the PA [1, 11] and, finally piezo-inertial drives, the movement of which is determined by the ratio between the friction force and the inertia force [12–15]. Inertial stepper piezoelectric drives, which will be called below as inertial drives (ID) for simplicity, are based on the electromechanical system consisting, as a rule, of a PA and a slider sliding along the rod. There are ID in which the PA is connected to a fixed base or moves along with the slider [16]. In this paper, the first option is considered. A qualitative explanation of the effect of moving the slider along the rod is based on the fact that the slider with a mass of M located on the rod moves with it during the smooth movement of the rod and slips due to inertia with a sharp acceleration of the rod. Thus, by applying asymmetric voltage control pulses with slow and fast fronts to the PA, leading to a slow elongation (compression) of the PA and subsequent rapid compression (elongation) to its original size, it is possible to move the slider step by step along the rod. There are known ID with both horizontal and vertical rod arrangement, having the same operating principles and differing in the fact that in the vertical ID, there is an additional clamping of slider to the rod. The stage of movement, when the slider moves along with the rod, and their relative velocity is zero, has a stable term in the literature – Stick (sticking). The stage when the relative velocity of the rod and slider is different from zero and slippage occurs has the term Slip. The paper considers an ID with a vertical rod arrangement. The reason is as follows. When moving up and down along the axis of the rod, only gravity and friction force F_{fr} act on the slider, its acceleration in the up direction a_{up} and in the down direction a_{down} in the inertial coordinate system (ICS) relative to the fixed base is determined by expressions (2) and (2), respectively:

$$a_{\text{up}} = \frac{F_{\text{fr}}}{m_{\text{slider}}} - g = \frac{\mu F_{\text{clamp}}}{m_{\text{slider}}} - g, \tag{1}$$

$$a_{\text{down}} = \frac{F_{\text{fr}}}{m_{\text{slider}}} + g = \frac{\mu F_{\text{clamp}}}{m_{\text{slider}}} + g, \tag{2}$$

$$F_{\text{fr}} = \mu N = \mu F_{\text{clamp}}, \tag{3}$$

where m_{slider} is the slider mass, N is the reaction force of the support, μ is the coefficient of friction, g is the acceleration of gravity, F_{clamp} is the clamping force.

As follows from these expressions, the amount of slider acceleration in the ISC is limited. Thus, the slider can move up or down with the rod (Stick phase) only if the acceleration value of the rod does not exceed the threshold values of the air, or down, and, as follows from the expressions (1, 2), $a_{\text{up}} < a_{\text{down}}$. If the absolute value of the rod acceleration exceeds the threshold value, then the slider will slip along the rod (Slip phase) [17, 18]. When slipping, the slider has a velocity in a non-inertial coordinate system (NICS) relative to the rod, directed opposite to the acceleration of the rod in the ICS. At all times when the rod is moving, the frictional force acting on the slider is a thrust force for it. This fact is important for understanding the nature of the slider movement. Of course, the quantitative ID model must take into account the detailed shape of the control pulses, the mechanical resonant frequency of the structure, the friction force in the rod-slider pair, and energy losses in the "PA-rod-slider" oscillatory electromechanical system. In [15], a study of the operation of the ID was conducted and it was shown that the trajectory of the slider depends on a combination of various factors. In [19, 20], the influence of the shape of the pulse on the movement of the slider was investigated. In [18, 21], the attention is paid to trajectories containing sections where the slider moves in the direction opposite to the direction of movement of the rod and the results of modeling of such trajectories are presented. It was shown in [22] that the ID can work even under the control of symmetric control pulses. Note that in some cases, for example, when moving over long distances, it is important to have a relatively high speed of the slider moving under the action of a sequence of pulses. To increase the ID speed, it is necessary to minimize the intervals between the control voltage pulses. However, with an increase in the frequency of repetition of control pulses, it is necessary to take into account the finiteness of the relaxation time of vibrations arising in the electromechanical system in response to a sharp excitation from a short front of the control pulse. The presence of vibrations was already noted in one of the first works on ID [23]. Vibrations caused by strong high-frequency harmonics of sawtooth and cycloidal control signals were noted in [24]. These vibrations affect the movement of the slider under the control of a sequence of pulses, but they can be ignored if the vibrations fade out in the time intervals between pulses [25]. Therefore, for the stable operation of the precision displacement system, it is necessary to coordinate the frequency of the control pulses with the attenuation time of vibrations occurring in the ID. Thus, despite the simplicity of the design and ease of operation, the trajectory of the slider in the ID can have a rather complex appearance, since it depends on many factors. It is clear that in order to carry out movements in increments of several tens of nanometers, which, generally speaking, corresponds to a distance separating only about a hundred atoms in a solid, a special "smart setting" of the ID is required. At the same time, it is useful to have preliminary calculated data obtained on the basis of an adequate model of a real ID [13, 26].

In this paper, we build the model, and use it for investigation the trajectories of movement of the rod and slider in the ICS (relative to a fixed base) and the trajectory of movement of the slider in the NICS (relative to a fixed rod). We also calculate the step value of the real ID depending on the amplitude and shape of the sawtooth control pulse and the clamping force of the slider to the rod. Also, the step value of the real ID is measured experimentally, depending on the shape of the control pulse and the calculated data are compared with experiment.

2. The design of the inertial stepper piezoelectric drives and the scheme of the experiment

The appearance and layout of the vertical ID are shown in Fig. 1(a,b,c), respectively.

A titanium rod (2) is fixed on the PA (1), to which a slider (3) is pressed. In cross-section, the rod has the shape of a triangle (Fig. 1(c)). The slider surface, which has the shape of a two-sided angle, is pressed against two flat surfaces of the corresponding dihedral angle on the rod using an elastic clamp (4) mounted on the slider. A fluoroplastic washer is installed in the contact area of the elastic element with the rod to reduce friction, so that the main friction acts between the surfaces of the rod and the slider. The slider design consists of several parts. The part of the slider in contact with the rod is made of titanium. Due to the triangular shape of the rod, the slider has one degree of freedom and can only move along the axis of the rod. A multilayer piezoelectric package (PP) (Pst150/5×5/7H) was used as a surfactant. The rod is connected to the PP through a thin layer of epoxy glue.

The general scheme for measuring the steps of the ID is shown in Fig. 2. To control the PP, a simple scheme for forming sawtooth control pulses based on an electronic key in the form of a field-effect transistor is used, the input of which is supplied with a sequence of rectangular pulses (Fig. 3). In the initial state, for the voltage at the input of the circuit $V = 0$, the transistor is closed, the capacitance of the PP is charged to a voltage $V_0 = 50$ V, and the PP is stretched by $3.5 \cdot 10^{-6}$ m. Under the action of an initial rectangular pulse with a voltage of $V = 12$ V and a duration of t_0, the transistor opens, and the PP is discharged to zero, passing into the initial equilibrium state. Here t_1, t_2 are

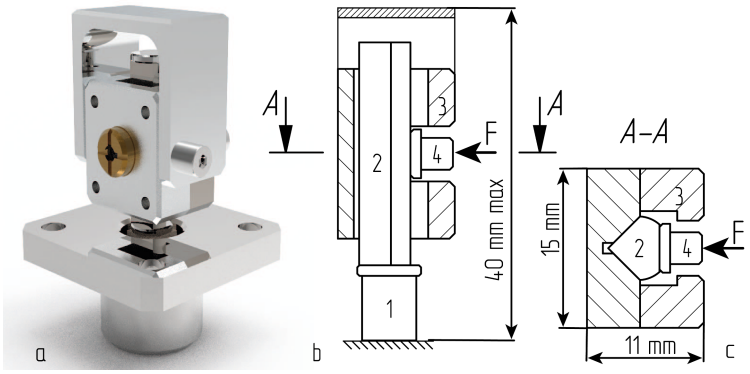

FIG. 1. Appearance (a) and the scheme of the inertial nano step piezoelectric drive (b – front view, c – top view) 1 – piezo package, 2 – rod, 3 – slider, 4 – clamp

the times set for the formation of a control sawtooth pulse with long leading and short trailing edges. Under the action of the leading edge, the PP slowly lengthens, and under the action of the trailing edge, it quickly contracts, returning to an equilibrium position. To reverse the direction of movement of the slider, switching is provided (not shown in the diagram) of the contacts at the input of the PP, leading to slow compression and rapid return of the PP to an equilibrium state. When the transistor is closed, the PP with its own capacity of $\sim 0.7 \cdot 10^{-6}$ F is charged through the resistance $R_1 = 2000$ ohms, and when the transistor is open, the PP is discharged through the resistance R_2. Using such a simple scheme, it is possible to control the step of the ID by changing the charging time of the PP t_1, or changing the time of its discharge by changing the resistance R_2. In our experiment, the resistance of R_2 varied from 1 ohm to 30 ohms. With a sharp voltage jump from 50 V to zero and a corresponding sharp compression of the PP in the PP-rod oscillatory system, damped resonant vibrations occur, depending on the quality factor of the system, and, thanks to the piezoelectric effect, there will be mutual influence of mechanical and electrical vibrations. The time t_0 required for relaxation of resonant vibrations and the transition of PP to an equilibrium state was determined experimentally and was ~ 2 ms. After the PP is transferred to an equilibrium state, the piezoelectric package is charged during time t_1. In our experiment, the time t_1 was 0.4 ms and 0.14 ms, which corresponded to the amplitude of 14 V and 5 V for the control sawtooth voltage pulse. Since the charging time constant is as follows: $\tau_1 = R_1 C \gg t_1$, the leading edge of the voltage pulse on the PP has a close to linear dependence on time, which leads to a corresponding smooth movement of the rod. The trailing edge is formed when the capacitance of the PP is discharged through the resistance R_2 when the transistor is opened for the time t_2. If the capacitance of the PP had a purely electrical nature, then its charging or discharging would not be accompanied by mechanical compression or stretching, and the trailing edge of the pulse would decay exponentially with a time constant $\tau_2 = R_2 C = (1 \div 30) \cdot 10^{-6}$ s. However, as mentioned above, it is necessary to take into account the emerging resonant vibrations, the attenuation of which will depend on the Q-factor of the oscillatory piezo electromechanical system. Using simulation, it will be shown below how the shape of the trailing edge depends on the resistance R_2, which affects both the discharge time of the PP and the Q-factor of the "PA-rod" oscillatory system.

Measurements of the ID step were carried out using the scanning probe microscopy (SPM) method. For this purpose, the ID was included in the "home-made" SPM as a system for approaching the probe with the sample. The sample had a smooth surface (roughness less than 1 nm) and was fixed on a slider. To measure the step value, the interaction between

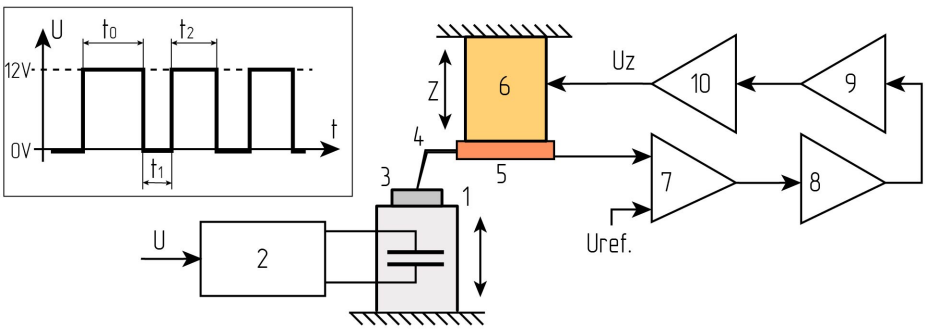

FIG. 2. Diagram of the experiment on measuring the value of the ID step. 1 – inertial piezo drive, 2 – sawtooth pulse control circuit, 3 – sample, 4 – probe, 5 – probe sensor, 6 — SPM scanner, 7 – differential amplifier, 8 – integrator, 9 – amplifier, 10 – high voltage amplifier

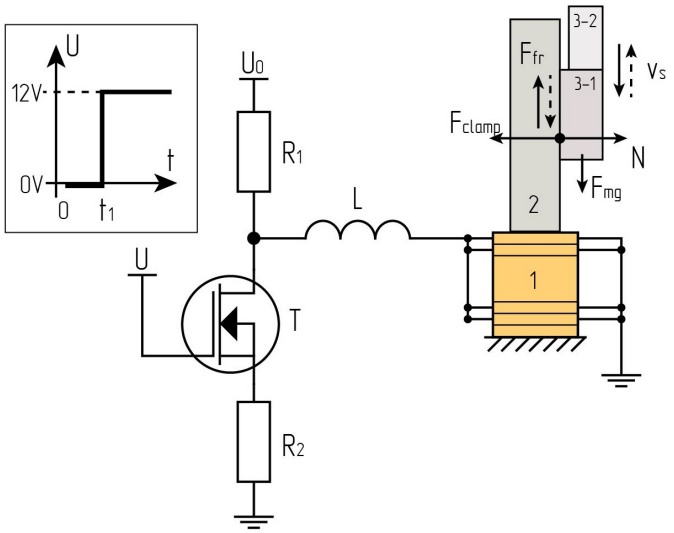

FIG. 3. Scheme of the ID calculation model 1 – piezo package, 2 – rod, 3-1 – slider (part in contact with the rod), 3-2 – slider (part without contact with the rod)

the probe and the sample was captured, after which the feedback in the SPM tracking system was broken, and the probe was withdrawn from the sample surface. Then the ID took a step, the tracking system turned on again, and the interaction was re-captured. The step length h was measured at the same interaction signal between the probe and the sample as the difference in positions of the SPM scanner before and after moving the ID under the action of a single control pulse [14]

$$h = \alpha \left| U_{Z_{n+1}} - U_{Z_n} \right|, \tag{4}$$

where α is the sensitivity of the SPM scanner, U_{Z_n} is the voltage on the SPM scanner after the (n)-th step of the slider, $U_{z_{n+1}}$ is the voltage on the SPM scanner after the $(n+1)$-th step. To measure the average value of a single step, multiple one-step movements were performed under the action of a sequence of control pulses and a histogram of the size distribution of steps was constructed. At the same time, the time t_2 was set so that the ID had time to relax after executing the next step.

3. Description of the model

Figure 3 shows the ID model investigated by the finite element method using the COMSOL software package. Since the slider moves only along one (vertical) spatial Z axis, a two-dimensional simplification of the three-dimensional problem is considered. The model includes a multilayer PP Pst150/5×5/7H and a sawtooth control pulse generation circuit based on an n-type MOSFET field-effect transistor. The parameters of the transistor were chosen so that the calculated shape of the control sawtooth pulse most closely corresponded to the shape of the real pulse, which was observed in the experiment when charging and discharging a conventional electrical capacitance equal in value to the capacitance of the used PP ($C = 0.7$ μF). At the same time, the values of the main parameters corresponded to the default parameters set in COMSOL, and the values of the parameters "Gate Length" and "Transconductance Parameter" were selected to be $1 \cdot 10^{-7}$ m and $2 \cdot 10^{-3}$ A/B^2, respectively. The package consists of 40 layers of piezoceramic material PZT 5H with a thickness of 0.17 mm, connected in parallel. The physical parameters of the PZT 5H were selected in the COMSOL library. In this case, the value of the piezoelectric module $e_{33} = 72$ Kl/m^2 was set based on the data specified by the manufacturer in the PP passport. The inductance $L = 2 \cdot 10^{-6}$ H is also included in the electrical circuit. The inductance $L \sim 1 \cdot 10^{-6}$ H is also included in the model, due to the conductive electrodes between the PP layers and the conductive wires in the electrical circuit. The value of this constructive inductance was estimated from an experimentally measured frequency $f \sim 200$ kHz in an electromagnetic oscillatory circuit with a known capacitance $C = 0.7 \cdot 10^{-6}$ F.

For a two-dimensional simulation of a three-dimensional slider, in the construction of which different materials (titanium and steel) are used, the slider is made up of two parts rigidly connected to each other. The material of the part in contact with the rod has all the properties of titanium, as does the rod. The density of the second part of the slider is set so that the total weight of the slider is 10 g, which corresponds to its real weight. The titanium rod is rigidly connected to the PP. The size of the rod and its weight embedded in the model correspond to the actual design of the ID. The slider is pressed against the rod by an elastic element with the force of F_{clamp}. Dry friction contact interaction is enabled between the surface of the rod and the slider. The friction at the point of contact of the elastic element with the surface of the rod is neglected, since it is much less than the friction in contact of the slider with the rod. The rod and slider are modeled as linear elastic materials, the calculations take into account the density, Young's modulus and Poisson's ratio for each material.

The ID model (Fig. 3) consists of a composition of several physical Comsol modules. The PP model is built using the modules "Solid Meshes" and "Electrostatics" using a multiphysical combination of these modules "Piezoelectric Effect". The finite element method was used to calculate both the deformation field at each point of the model grid and the electric field in the PP. The model of an electric circuit built with the help of the "Electrical Circuit" module using the "Terminal" mechanism fully reproduces the electrical circuit shown in Fig. 3. The step pulse with a height of 12 V is supplied at the input of circuit, and the time interval t_1 ($t_1 \ll R_1C$) before the start of the voltage surge corresponds to the time of the open state of the transistor, when the PP is charging, and sets the amplitude of the control sawtooth pulse. The models of the rod, slider and contact interaction between them are made using the "Multibody Dynamics" module. At the same time, a rigid connection of the rod and the PP is implemented using the "Fixed Joint" element. For the rightmost border of the rod and the leftmost border of the slider, a "Prescribed displacement" offset constraint is set along the horizontal axis. The introduction of this restriction is due to the rigidity of the actual ID design. The contact interaction between the rod and the slider is modeled based on the condition that the movement of the touching bodies occurs along one spatial axis (vertical). Due to the limited information on contact interaction, the most generalized method of describing contact was chosen using a lumped connection of the prismatic type "Prismatic Joint", in which the movement of contacting bodies is allowed only along one direction and any turns are prohibited.

The following equations were solved jointly:

1. The equation of motion in a form that takes into account mechanical vibrations in the system

$$\rho\frac{d^2x}{dt^2} - \rho\omega^2 x = \nabla \cdot S, \tag{5}$$

   where S is the stress tensor, $\omega = 2\pi f_0$, where f_0 is the mechanical resonance frequency.
2. Linear elasticity equation (linear relationship between mechanical stress and strain)

$$S = c : \varepsilon, \tag{6}$$

   where c is the stiffness matrix, ε is the strain tensor. Deformations are considered as engineering, which is an acceptable approximation when linear changes in the size of objects are relatively small.
3. The electric field is additionally calculated for PP

$$\mathbf{E} = -\nabla V, \tag{7}$$

$$\nabla \cdot (\varepsilon_0\varepsilon_r\mathbf{E}) = \rho_v, \tag{8}$$

   where $\mathbf{E}$ is the vector of the electric field, V is the electric potential, ε_r is the dielectric constant of material, ε_0 is the dielectric constant of vacuum, ρ_v is the spatial charge density.
4. Equation for the dry friction force

$$F_{\text{fr}} = -\mu N\frac{v}{|v|}\left(1 - \exp\left(-\frac{|v|}{v_0}\right)\right), \tag{9}$$

   where v is the velocity of the slider relative to the rod, μ is the coefficient of friction, N is the normal reaction force of the support, v_0 is the velocity, the value of which is small compared to the velocities in the system. The minimum velocity v_0 is introduced to ensure the continuity of the function by which the friction force is calculated. This eliminates the mathematical problem associated with the discontinuity of the slider speed during the transition from the sticking phase to the sliding phase. Considering that the minimum slider speed in our case is $\sim 10^{-4}$ m/sec, the value for v_0 was $\sim 5 \cdot 10^{-5}$ m/sec. The above formulation is the law of continuous friction and describes both slip and stick, and thus completely replaces Coulomb's law. Sticking is replaced by sliding between touching bodies with a small relative velocity. This explains the slight slope of the slider trajectory $X(t)$, which always takes place under the influence of gravity. Therefore, within the framework of this model, the resulting step is calculated at the moment when the slider speed relative to the rod becomes less than v_0.
5. Equations describing the piezo effect in the "Stress-Sharge" formulation

$$T = c^E S - e_t\mathbf{E}, \tag{10}$$

$$\mathbf{D} = e_t S + \varepsilon_0\varepsilon^S\mathbf{E}, \tag{11}$$

   where T is the mechanical stress tensor, S is the strain tensor, $\mathbf{D}$ is the electric displacement field (induction), et is the relationship matrix (piezomodule), c^E is the stiffness matrix, e^S is the relative permittivity matrix. The values of the main parameters of the ID model are presented in Table 1.

TABLE 1. The main parameters of the ID model

Name	Value	Units of measurement
PP dimensions	$9 \times 5 \times 5$	mm
Rod dimensions	$25 \times 5 \times 5$	mm
Slider mass	10	g
Clamp force	1.2	N
Friction coefficient	0.25	
Charge resistance R_1	2000	Ω
Discharge resistance R_2	1 – 30	Ω
Young's modulus of PP (c_{33}^E)	117	GPa
Piezo module of PP (e_{33})	72	C/m^2
Density of PP	7500	kg/m^3
Young's modulus of titanium	112	GPa
Poisson's ratio of titanium	0.32	
Density of titanium	4505	kg/m^3
Young's modulus of steel	200	GPa
Poisson's ratio of steel	0.3	
Density of steel	7850	kg/m^3
Voltage V_0	50	V
PP charging time (t_1)	0.4, 0.14	ms

4. Simulation results, comparison with experiment

Let's analyze the dependence of the slider trajectory and the step size on the shape of the control pulse in the case of slider steps direction upward. Fig. 4(a,b) shows the shape of the control voltage pulse at the input of the PP for various resistance values R_2. Fig. 5(a,b) show the trajectories of the rod and slider, respectively, in the ICS relative to the fixed base. As mentioned above, a small slope in the dependence of the slider offset on time, which occurs after the end of the control pulse in the ICS (Fig. 5(b)), should not be taken into account, since it is an artifact of the model. Figs. 6(a,b) show the speed of the slider and the movement of the slider, respectively, in NICS (with relation to a rod). Under the action of a linearly increasing leading edge (Fig. 4(a)), the PP linearly expands, which leads to a smooth linear movement of the rod upwards in the ICS by ~ 800 nm (Fig. 5(a)) with acceleration and deceleration at the beginning and at the end of the linear movement, causing a slip phase. Slippage leads to the fact that the slider lags behind the rod and has a nonlinear dependence of movement on time (Fig. 5(a)). As can be seen from Fig. 6(b), the slider descends downwards relative to the fixed rod by ~ 600 nm. As a result, under the action of the slow leading edge of the sawtooth voltage, the slider rises only by ~ 200 nm in the direction of the fixed base (Fig. 5(b)).

Changing the resistance of R_2 changes the constant τ_2 and affects the shape of the trailing edge of the control pulse. At small resistances R_2 (1 and 5 ohm), there is a rapid discharge of the PP capacitance, which leads to its sharp contraction, causing the excitation of electromechanical resonance oscillations with exponentially decaying amplitude in the system "PP-rod". Fig. 5(a) observes the resonant oscillations of the rod at 30 kHz, while Fig. 4(b) shows the corresponding voltage oscillations on the PP. The resonant oscillation of the rod produces slip, which is confirmed by the appearance of the slider's velocity relative to the stationary rod in the NICS (Fig. 6(a)). The change in sign of velocity observed in Fig. 6(a) means that the slider slips both up the rod (positive sign of velocity) and down the rod (negative sign). For example, with $R_2 = 1$ ohm, when the rod is first sharply lowered downward maximally, the slider moves upward maximally by ~ 1400 nm relative to the stationary rod due to slip. Then, as a result of several oscillations of the rod with damped amplitude, the slider periodically slips up and down the rod, dropping to ~ 650 nm (Fig. 6(b)), and stops at ~ 110 nm above the fixed base in the ICS, i.e., the resulting step of slider movement is ~ 110 nm. Note that in the case of fast discharge of the PP and low losses in the discharge circuit ($R_2 = 1$ and 5 ohm), the voltage on the PP changes sign, (Fig. 4(b)) and the rod passes through the equilibrium position in the ICS during oscillation (Fig. 5(a)).

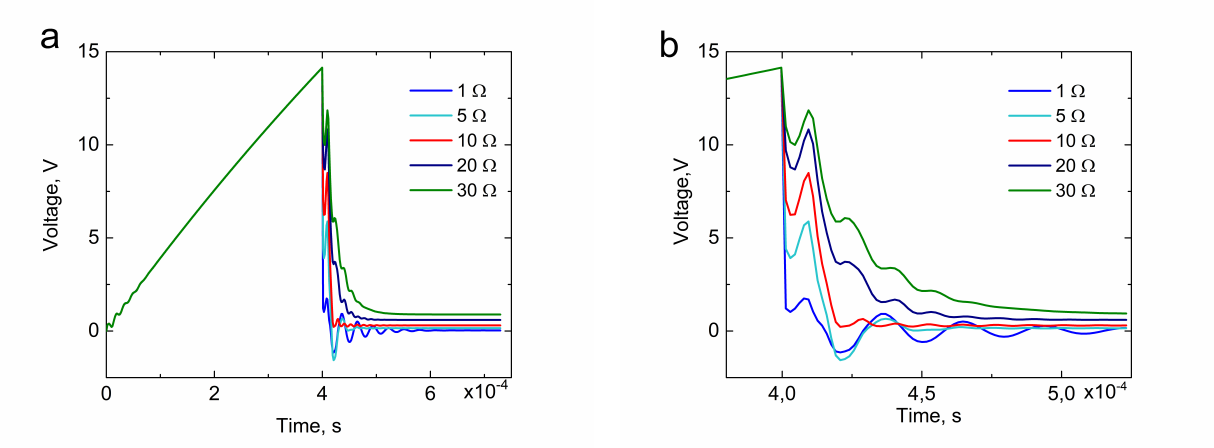

FIG. 4. The shape of the control voltage pulse at various resistances R_2. a – is the entire pulse, b – is the time-stretched trailing edge of the pulse

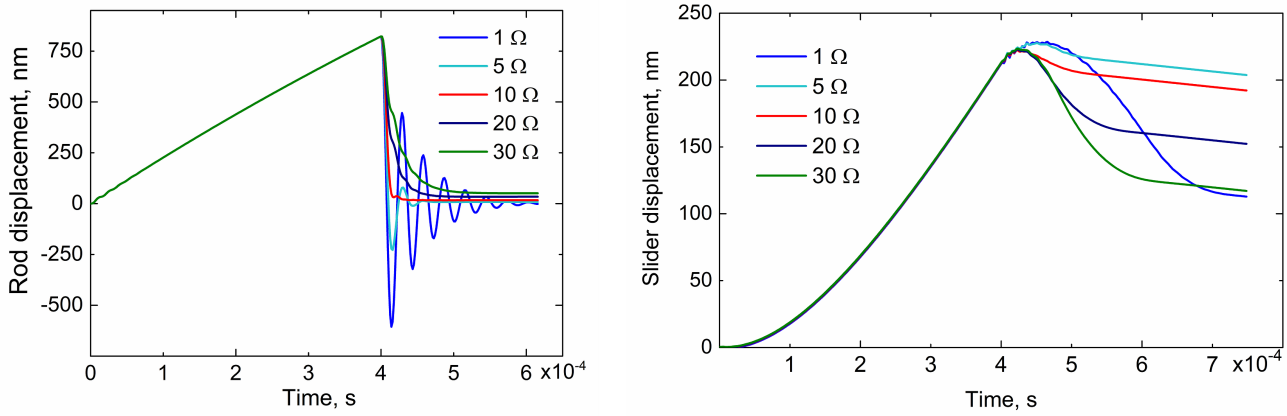

FIG. 5. Movement of the rod (a) and slider (b) in the ICS relative to the fixed base at different resistances R_2

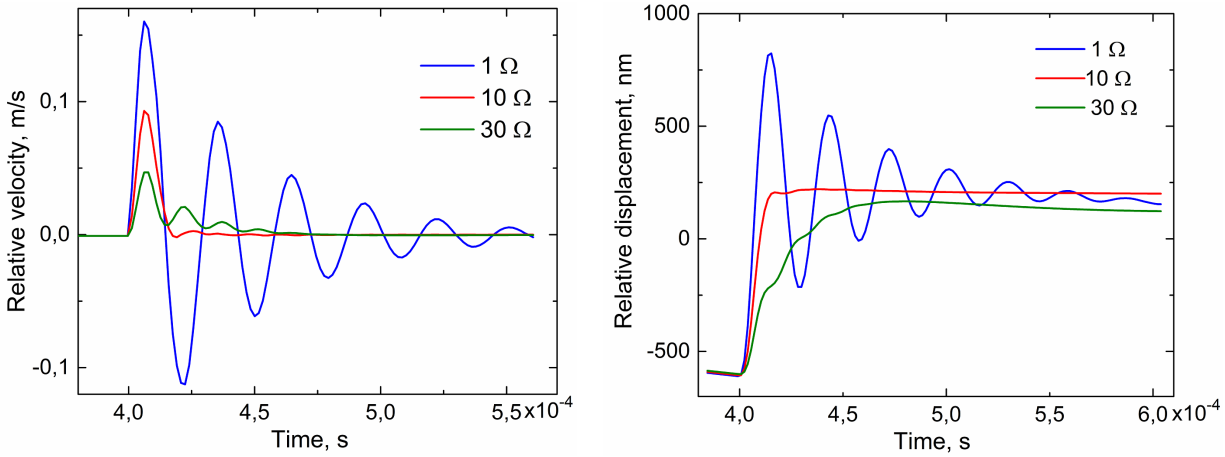

FIG. 6. The speed (a) and movement (b) of the slider in ICS relative to a fixed rod at various resistances R_2

When R_2 is increased (10, 20, 30) ohms, the character of the change in the voltage across the PCB and the rod displacement changes. Now there are no oscillations and there is an exponential in time decrease of the voltage on the PCB and corresponding exponential in time displacement of the rod to the equilibrium position (Figs. 4(b), 5(a)). The exponential decline is explained, firstly, by the fact that as the resistance increases, the Joule losses in the PP discharge circuit also increase and, consequently, the goodness of the piezo electromechanical oscillating system decreases. Second, as R_2 increases, the discharge time constant τ_2 increases, and the PP contracts more smoothly, so that resonant oscillations with appreciable amplitude are not excited, or are quickly damped. We attribute the observed steps on the exponential tails to the manifestation of the piezo effect. As can be seen from Fig. 6(a), in this case the slider velocity does not change sign and the slip is only one way up the rod without oscillation. At resistance $R_2 = 30$ ohm, under the action of the trailing edge of the control pulse, the slider acquires a velocity in NICS relative to the stationary rod, which, however, does not change sign, and slippage occurs only one way up the rod without oscillation. As a result, under the action of a fairly smooth trailing edge ($R_2 = 30$ ohm) when the rod is lowered, the slider slips ~ 700 nm up the rod (Fig. 6(b)) and stops ~ 120 nm above the fixed base in the NICS (Fig. 5(b)). Thus, despite the different nature of slider movement along the rod at $R_2 = 1$ ohm and $R_2 = 30$ ohm, the resulting slider pitch appears to be approximately the same and equal to 110 and 120 nm, respectively. In the case of $R_2 = 10$ ohm, due to a rather sharp voltage drop on the PP (Fig. 4(b)) and a sharp downward movement of the rod without oscillations in the ICS (Fig. 5(a)), there is a strong slip of the slider up the rod by ~ 800 nm (Fig. 6(b)) practically without rolling down, so that the resulting slider step has a value equal to ~ 200 nm (Fig. 5(b)).

We consider the optimal trajectory of the slider to be one where there is no oscillation of the slider relative to the rod and the time for the rod to return to the equilibrium state is minimized. Indeed, the absence of oscillations reduces the length of the trajectory of the slider movement along the rod and, consequently, reduces wear and heating of the surface, and the reduction of the relaxation time allows to reduce the intervals between steps, which is important for increasing the movement speed. In our case, as can be seen from Figs. 5,6, the optimum trajectory takes place when the resistance is as follows: $R_2 = 10$ ohm. Fig. 7 shows the histogram of the distribution of the value of ID steps obtained at the optimal trajectory of the slider.

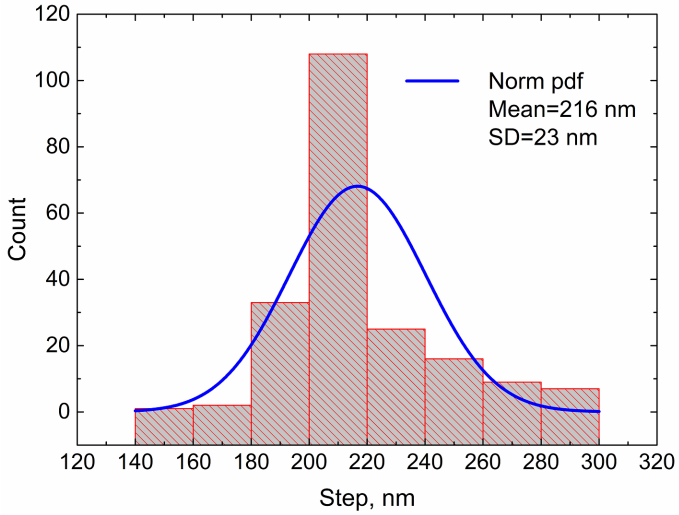

FIG. 7. Histogram of the distribution of ID steps at $R_2 = 10$ Ohm

Figure 8 shows the calculated and experimental curves obtained for the slider pitch value as a function of resistance R_2. It can be seen that the calculated and experimental curves have close maximum values, $h = 220$ nm at $R_2 = 7$ ohm and $h = 205$ nm at $R_2 = 10$ ohm, respectively, which confirms the adequacy of the constructed model.

Figure 9 demonstrates the trajectory of the slider in the ICS relative to the fixed base as a function of the clamping force. It can be seen that when the clamping force increases, the slip of the slider on the slow edge of the sawtooth control pulse decreases and the slider practically does not lag behind the displacement of the rod in the ICS. Indeed, at a clamping force of 120 g, the slider moves ~ 200 nm in the ICS relative to the fixed base (Fig. 9), while the rod moves ~ 800 nm (Fig. 5(a)), indicating that the slider lags significantly behind the rod as a result of slippage. However, at a clamping force of 400 g, the slider practically moves with the rod as its displacement is ~ 800 nm (Fig. 9), indicating negligible slippage. At the same time, the displacement step also increases from ~ 200 to ~ 800 nm. Thus, we can see that by increasing the clamping, it is possible to reduce the slip under the action of the slow edge of the control pulse and to increase the length of the ID step. Of course, it should be remembered that increasing the pressure increases the wear of the rubbing surfaces, which can impair the reproducibility of the ID steps. In addition, increasing the pressure will reduce the slippage under

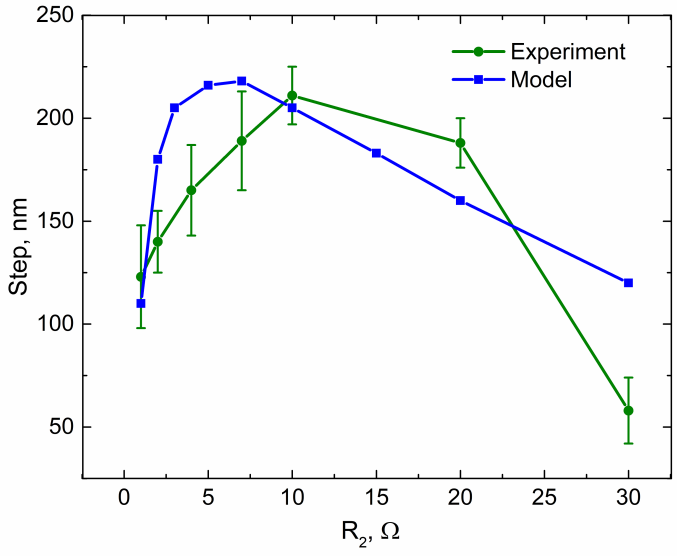

FIG. 8. Model and experimental plots of the dependence of the slider step size on the resistance R_2 in the PA discharge circuit

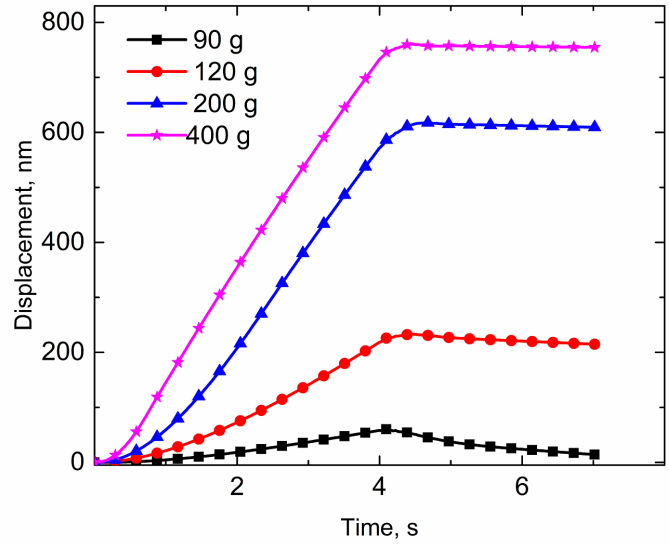

FIG. 9. Trajectories of the slider in the ICS relative to the stationary base at different pressing force

the action of the fast trailing edge, which will reduce the value of the ID step, and if the pressure is too high, it will stop the operation of the ID altogether.

The slider displacement step can also be controlled by changing the amplitude of the sawtooth voltage of the control pulse. Fig. 10 shows the results of calculating the rod, slider and slider displacement step size in the ICS with resistance $R_2 = 10$ ohm, but under the action of a sawtooth control pulse with a smaller amplitude, formed by decreasing the time t_1 from 0.4 to 0.14 ms. It can be seen that reducing the amplitude of the control sawtooth pulse from 14 to 5 V results in a decrease in the step size from ~ 200 to ~ 30 nm.

5. Results and conclusions

The design and numerical model of a vertical ID controlled by sawtooth voltage pulses with slow leading and fast trailing edges are proposed. The control pulses are generated by a simple circuit based on an electronic key by charging/discharging the electrical capacitance of the PA at a large charge time constant and a small discharge time constant. Using the finite element method, the trajectories of the rod and slider movement and the step size of the vertical ID depending on the amplitude and shape of the sawtooth-shaped control pulse and the force of the slider pressure on the rod are investigated. It is found that inertial slippage in the friction pair "slider-rod" occurs both at the fast and slow fronts of the control pulse. A piezo electromechanical resonance in the system "PA-rod-slider", which is excited by a sharp discharge of PA capacitance and causes harmful oscillations of the slider, is detected. It is shown that it is possible to eliminate

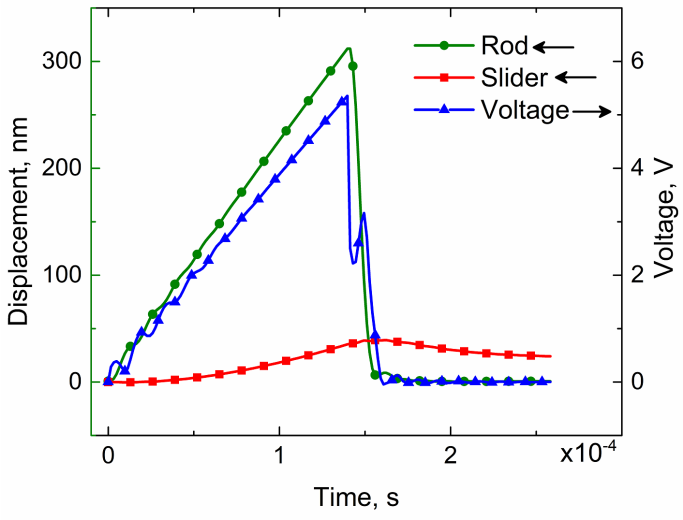

FIG. 10. Trajectories of rod and slider motion in the ICS relative to the fixed base under the action of the control sawtooth voltage pulse with amplitude ~ 5 V

resonance oscillations by selecting the optimum value for the resistance in the PA discharge circuit, which affects both the discharge rate and the goodness of the piezo electromechanical resonator. It is shown that, with the optimal resistance in the PA discharge circuit, it is possible, by changing the charge time and the pressure force, to control the slider movement step during its progressive upward movement along the guide rod without rolling back. The magnitude of the actuator step as a function of the resistance in the PA discharge circuit is experimentally measured. A satisfactory agreement between the calculated and experimental data in the nanometer range of the ID displacements was obtained, which confirms the adequacy of the proposed model. The obtained results can be used in the development and tuning of ID.

References

[1] Spanner K., Koc B. Piezoelectric Motors, an Overview. *Actuators*, 2016, **5**, 6.
[2] Bobtsov A.A., Boykov V.I., Bystrov S.V., Grigoriev V.V., Karev P.V. *Actuators and systems for micromovements: textbook*. ITMO University, SPb, 2017, 134 p.
[3] Mohith S., Upadhya A.R., Navin K.P., Kulkarni S.M., Rao M. Recent trends in piezoelectric actuators for precision motion and their applications: a review. *Smart Materials and Structures*, 2021, **30** (1), 3002.
[4] Wang L., Chen W., Liu J., Deng J., Liu Y. A review of recent studies on non-resonant piezoelectric actuators. *Mechanical Systems and Signal Processing*, 2019, **133** (1), 106254.
[5] Bansevicius R., Ragulskis K. *Vibromotors*. MOKSLAS Publishing House, Vilnius, Lithuania, 1981, 170 p. (In Russian)
[6] Ragulskis K., Bansevicius R., Barauskas R., Kulvietis G. *Vibromotors for Precision Microrobots (Application of Vibration Series)*, Hemisphere Publishing Co., Detroit, 1988, 310 p.
[7] Ueha U., Tomikawa Y. *Ultrasonic Motors: Theory and Applications*. Clarendon: Oxford, UK, 1993, 297 p.
[8] Sashida T., Kenjo T. *An Introduction to Ultrasonic Motors*. Clarendon: Oxford, UK, 1993, 254 p.
[9] Uchino K. *Piezoelectric Actuators and Ultrasonic Motors*. Boston, MA: Kluwer Academic Publisher, USA, 1997, 347 p.
[10] Zhao C. *Ultrasonic Motors: Technologies and Applications*. Science Press: Beijing, China; Springer Verlag: Berlin, Germany, 2011, 494 p.
[11] Müller K.D., Marth H., Pertsch P., Gloess R., Zhao X. Piezo-Based, Long-Travel Actuators for Special Environmental Conditions. *Proceedings of the 10th Int. Conference on New Actuators*, Bremen, Germany, 14 – 16 June 2006, P. 149 – 153.
[12] Golubok A.O., Timofeev V.A. STM Combined with SEM without SEM Capability Limitations. *Ultramicroscopy*, 1992, **42–44** (2), P. 1558–1563.
[13] Koc B., Delibas B. Impact Force Analysis in Inertia-Type Piezoelectric Motors. *Actuators*, 2023, **12**, 52.
[14] Gorbenko O.M., Zhukov M.V., Pichakhchi S,V., Sapozhnikov I.D., Felshtyn M.L., Golubok A.O. Compact Scanning Probe Microscope Head Based on Inertial Trusters Using Piezopakets. *Nauchnoe Priborostroenie*, 2021, **31** (2), P. 3–22.
[15] Hunstig M. Piezoelectric Inertia Motors – A Critical Review of History, Concepts, Design, Applications, and Perspectives. *Actuators*, 2017, **6**, 7.
[16] Liu P.,Wen Z., Sun L. An In-Pipe Micro Robot Actuated by Piezoelectric Bimorphs. *Chin. Sci. Bull.*, 2009, **54**, P. 2134–2142.
[17] Okamoto Y., Yoshida Y. Development of linear actuators using piezoelectric elements. *Electron. Comm. Jpn.*, 1998, **81**, P. 11–17.
[18] Drevniok B., Paul W.M., Hairsine K.R., McLean A.B. Methods and instrumentation for piezoelectric motors. *Rev. Sci. Instrum.*, 2012, **83**, 033706.
[19] Wang J., Lu Q. How are the behaviors of piezoelectric inertial sliders interpreted? *Rev. Sci. Instrum.*, 2012, **83**, 093701.
[20] Gao Q., He M., Lu X., Zhang C., Cheng T. Simple and high-performance stick-slip piezoelectric actuator based on an a symmetrical flexure hinge driving mechanism. *J. of Intelligent Material Systems and Structures*, 2019, **30** (14), P. 2125–2134.
[21] Sun P., Xu Z., Jin L., Zhu X. A Novel Piezo Inertia Actuator Utilizing the Transverse Motion of Two Parallel Leaf-Springs. *Micromachines (Basel)*, 2023, **14** (5), 954.
[22] Renner C., Niedermann P. A vertical piezoelectric inertial slider. *The Review of scientific instruments*, 1990, **61** (3), P. 965–967.
[23] Pohl D.W. Dynamic Piezoelectric Translation Devices. *Rev. Sci. Instrum.*, 1987, **58**, P. 54–57.
[24] Dubois F., Belly C., Saulot A., Berthier Y. Stick-slip in stepping piezoelectric Inertia Drive Motors – Mechanism impact on a rubbing contact. *Tribology International*, 2016, **100**, P. 371–379.

[25] Zhang H., Zeng P., Hua S., Cheng G., Yang Z. Impact Drive Rotary Precision Actuator with Piezoelectric Bimorphs. *Front. Mech. Eng. China*, 2008, **3**, P. 71–75.

[26] Ceponis A., Jurenas V., Mažeika D., Bakanauskas V., Deltuviene D. Rod-Shaped Linear Inertial Type Piezoelectric Actuator. *Actuators*, 2023, **12**, 379.

Submitted 14 August 2024; revised 2 September 2024; accepted 3 September 2024

Information about the authors:

Olga M. Gorbenko – Institute for Analytical Instrumentation of RAS, St. Petersburg, Russia; ORCID 0000-0002-7054-6602; gorolga64@gmail.com

Stanislav Y. Lukashenko – Institute for Analytical Instrumentation of RAS, St. Petersburg, Russia; ORCID 0000-0002-5356-1261; lukashenko13@mail.ru

Stepan V. Pichakhchi – Institute for Analytical Instrumentation of RAS, St. Petersburg, Russia; St. Petersburg Academic University, St. Petersburg, Russia; ORCID 0000-0002-8578-5200; pichakhchi.s@yandex.ru

Ivan D. Sapozhnikov – Institute for Analytical Instrumentation of RAS, St. Petersburg, Russia; ORCID 0000-0003-2575-5015; sapojnikov@gmail.com

Mikhail L. Felshtyn – Institute for Analytical Instrumentation of RAS, St. Petersburg, Russia; ORCID 0000-0001-8677-061X; mfelsztyn@yandex.ru

Alexander O. Golubok – Institute for Analytical Instrumentation of RAS, St. Petersburg, Russia; St. Petersburg Academic University, St. Petersburg, Russia; ORCID 0000-0001-9970-9172; aogolubok@mail.ru

Conflict of interest: the authors declare no conflict of interest.